nature astronomy

LETTERS

PUBLISHED: 12 JUNE 2017 | VOLUME: 1 | ARTICLE NUMBER: 0146

Disk-driven rotating bipolar outflow in Orion Source I

Tomoya Hirota[1,2]*, Masahiro N. Machida[3], Yuko Matsushita[3], Kazuhito Motogi[4,5], Naoko Matsumoto[1,6], Mi Kyoung Kim[7], Ross A. Burns[8] and Mareki Honma[4,9]

One of the outstanding problems in star formation theory concerns the transfer of angular momentum so that mass can accrete onto a newly born young stellar object (YSO). From a theoretical standpoint, outflows and jets are predicted to play an essential role in the transfer of angular momentum[1–4] and their rotations have been reported for both low-[5] and high-mass[6,7] YSOs. However, little quantitative discussion on outflow launching mechanisms has been presented for high-mass YSOs due to a lack of observational data. Here we present a clear signature of rotation in the bipolar outflow driven by Orion Source I, a high-mass YSO candidate, using the Atacama Large Millimeter/Submillimeter Array (ALMA). A rotational transition of silicon monoxide ($Si^{18}O$) reveals a velocity gradient perpendicular to the outflow axis, which is consistent with that of the circumstellar disk traced by a high excitation water line. The launching radii and outward velocity of the outflow are estimated to be >10 au and 10 km s^{-1}, respectively. These parameters rule out the possibility that the observed outflow is produced by the entrainment of a high-velocity jet[8], and that contributions from the stellar wind[9] or X-wind[10], which have smaller launching radii, are significant in the case of Source I. Thus these results provide convincing evidence of a rotating outflow directly driven by the magneto-centrifugal disk wind launched by a high-mass YSO candidate[6,11].

Orion Source I is a radio-emitting young stellar object (YSO) candidate located in the Orion Kleinmann-Low (KL) region of the famous Orion nebula. As one of the nearest high-mass star-forming regions (418 pc from the Sun[12]), it is an ideal target for high-resolution observations. The $\sim 10^4 L_\odot$ central object[13–15] drives a low-velocity (~18 km s^{-1}) bipolar outflow along the northeast–southwest direction on a 1,000 au scale, oriented at an almost edge-on view[6,16,17]. At the centre of the outflow, vibrationally excited SiO masers trace a rotating outflow arising from the surface of a circumstellar disk with a radius of ~50 au[11,12], consistent with a magneto-centrifugal disk wind[6,11]. Recent high-angular resolution (100–200 au) Atacama Large Millimeter/Submillimeter Array (ALMA) observations of various molecular lines at high excitation energies of 500–3,500 K[18–21] revealed a rotating hot molecular gas disk with an enclosed mass of (5–7) $M_\odot$.

To reveal the interplay between disk accretion and outflow mechanisms in Source I, we present observational results with ALMA at 110–120 mas, or 50 au resolution (see Methods). Figure 1 shows integrated intensity and peak velocity maps of the 484.056 GHz $Si^{18}O$ ($J = 12–11$, where J is the quantum number of the total rotational angular momentum) and the 463.171 GHz H_2O ($\nu_2 = 1$, $J_{K_a,K_c} = 4_{2,2}–3_{3,1}$, where ν_2 is the vibrational quantum number in the bending mode and K_a and K_c represent projections of J onto the a and c inertial axes, respectively) lines, along with the continuum emission at 490 GHz[22]. The continuum emission has a deconvolved size of 90 au × 20 au extending perpendicular to the northeast–southwest bipolar outflow arising from the edge-on rotating disk[14,21–23]. The 484 GHz $Si^{18}O$ line clearly traces a northeast–southwest bipolar outflow, although the size of the outflow lobes, ~200 au, are much smaller than that traced by the lower energy transitions[16,17]. This is because the critical density required to excite the $J = 12–11$ transition (6×10^7 cm^{-3}) is higher than those of $J = 2–1$ at 86 GHz (3×10^5 cm^{-3})[16] and $J = 5–4$ at 217 GHz (4×10^6 cm^{-3})[17]. It is also expected that the optically thin, less abundant $Si^{18}O$ isotopologue ($^{16}O/^{18}O \approx 250$)[24] selectively traces regions of higher density than the optically thick $Si^{16}O$ lines. In contrast, the 463 GHz H_2O line shows a more compact structure than that of the $Si^{18}O$ map. Because of its high excitation energy (2,744 K), the 463 GHz H_2O line would be emitted from the hot molecular gas disk and the base of the outflow closer to the central YSO[19,21] than the 484 GHz $Si^{18}O$ line.

Both the 484 GHz $Si^{18}O$ and 463 GHz H_2O maps clearly show velocity gradients along the disk plane (Fig. 1b,c). Velocity gradients across the outflow or jet axis of other sources have been detected and have been attributed to rotation motions[5]. Alternative scenarios have also been suggested to explain the observed gradients, such as precessing motion, interaction with a warped disk, or two unresolved jets. However, we could not see any hints of a wiggled or S-shaped point symmetrical structure, or disagreement of the velocity structures in opposing outflow lobes or between the disk and outflow, unlike in previous studies. In contrast, we spatially resolve the velocity gradients in both lobes of the molecular outflow traced by the $Si^{18}O$ emission, which are similar in the observed H_2O emission (which traces the disk) (Fig. 2 and Supplementary Fig. 5). All the observed parameters and properties can be explained consistently

[1]Mizusawa VLBI Observatory, National Astronomical Observatory of Japan, Osawa 2-21-1, Mitaka-shi, Tokyo 181-8588, Japan. [2]Department of Astronomical Sciences, SOKENDAI (The Graduate University for Advanced Studies), Osawa 2-21-1, Mitaka-shi, Tokyo 181-8588, Japan. [3]Department of Earth and Planetary Sciences, Faculty of Sciences, Kyushu University, Motooka 744, Nishi-ku, Fukuoka-shi, Fukuoka 819-0395, Japan. [4]Mizusawa VLBI Observatory, National Astronomical Observatory of Japan, Hoshigaoka 2-12, Mizusawa-ku, Oshu-shi, Iwate 023-0861, Japan. [5]Graduate School of Sciences and Technology for Innovation, Yamaguchi University, Yoshida 1677-1, Yamaguchi-shi, Yamaguchi 753-8512, Japan. [6]The Research Institute for Time Studies, Yamaguchi University, Yoshida 1677-1, Yamaguchi-shi, Yamaguchi 753-8511, Japan. [7]Korea Astronomy and Space Science Institute, Hwaam-dong 61-1, Yuseong-gu, Daejeon 305-348, Republic of Korea. [8]Joint Institute for VLBI ERIC, Postbus 2, 7990 AA Dwingeloo, The Netherlands. [9]Department of Astronomical Sciences, SOKENDAI (The Graduate University for Advanced Studies), Hoshigaoka 2-12, Mizusawa-ku, Oshu-shi, Iwate, 023-0861, Japan. *e-mail: tomoya.hirota@nao.ac.jp

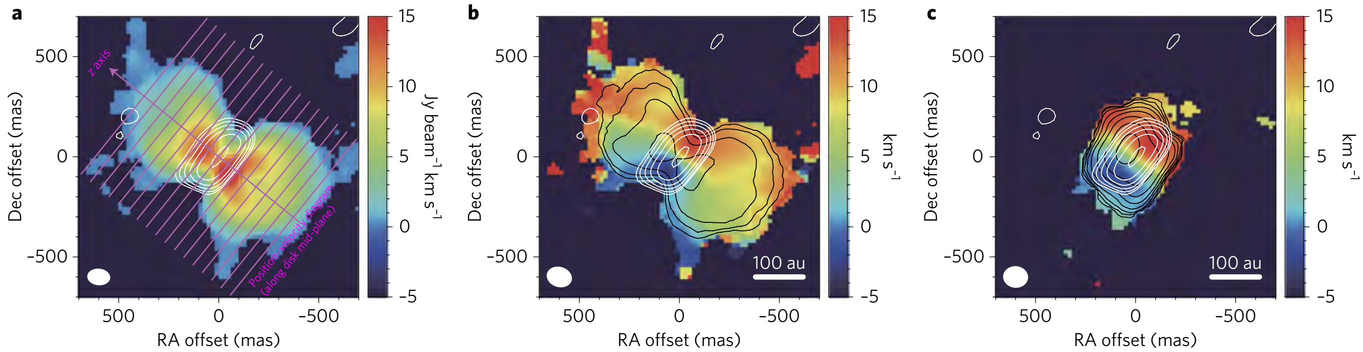

Figure 1 | Moment maps of the observed lines and continuum emissions. **a**, 490 GHz continuum (white contours) and moment 0 (integrated intensity; colour) maps of the 484 GHz $Si^{18}O$ line. **b**, 490 GHz continuum (white contours), moment 0 (black contours) and moment 1 (peak velocity; colour) maps of the 484 GHz $Si^{18}O$ line. **c**, 490 GHz continuum (white contours), moment 0 (black contours) and moment 1 (colour) maps of the 463 GHz H_2O line. Contour levels are 3, 6, 12, 24, … times the root mean square (r.m.s.) noise levels and the r.m.s. noise levels are 5 mJy beam^{-1}, 481 mJy beam^{-1} km s^{-1} and 56 mJy beam^{-1} km s^{-1}, respectively, for the continuum, moment 0 map of the $Si^{18}O$ line, and moment 0 map of the H_2O line. Synthesized beam sizes are indicated at the bottom-left corner of each panel. In **a**, the solid magenta lines indicate slices of the position–velocity diagram at 0, ±60, ±120, ±180, ±240, ±300, ±360, ±420 and ±480 mas from the disk mid-plane. The width of each slice is 60 mas. The interval of the slices parallel to the northwest–southeast direction is 60 mas, corresponding to $\Delta z = 25$ au at the distance of Orion KL. The northeast–southwest outflow axis is defined as z in Supplementary Fig. 4. The position angle of the slice is determined from the Gaussian fitting of the continuum emission. RA, right ascension; Dec, declination.

via the rotation motions of the disk and outflow. Thus we conclude that outflow rotation is the best explanation for the velocity gradients in Source I.

The signature of rotation is clearly demonstrated in the position–velocity diagrams of the 484 GHz $Si^{18}O$ and 463 GHz H_2O emissions in the disk mid-plane (Fig. 2a,b). These are analogous to those of the high excitation lines detected by recent ALMA observations[19,21]. The position–velocity maps exhibit a signature of a central hole (Supplementary Fig. 1b), suggesting that emission from the outer parts of the outflow is dominant and/or that high opacity continuum emission could obscure the innermost region in the mid-plane[19,21,22]. The inner (R_{in}) and outer (R_{out}) radii of the disk, and the rotation velocities at these positions, are derived from the $Si^{18}O$ map, $R_{in}(z=0) = 24 \pm 8$ au, $R_{out}(z=0) = 76 \pm 4$ au, $v_\phi(z=0, r=R_{in}) = 17.9 \pm 0.6$ km s^{-1} and $v_\phi(z=0, r=R_{out}) = 7.0 \pm 0.4$ km s^{-1} with 1σ errors (see Methods), where v_ϕ is the rotation velocity, r is the distance (au) from the rotation axis and z is the distance (au) from the mid-plane of the disk. Although these values can be explained by a rotation curve conserving angular momentum, $v_\phi \propto r^{-1}$, the position–velocity diagrams could not distinguish Keplerian rotation, $v_\phi \propto r^{-0.5}$ due to insufficient resolution. Assuming Keplerian rotation, the enclosed mass is estimated to be $8.7 \pm 0.6\ M_\odot$ (1σ) from the maximum rotation velocity at the inner radius. The result is consistent with the mass estimated from SiO maser observations[11]. However, the shallower velocity gradient around the systemic velocity (5 km s^{-1}) agrees with a smaller enclosed mass[19,21]. It is also likely that the inner radii and resultant enclosed mass could be overestimated due to insufficient angular resolution.

We made slices for position–velocity diagrams of the 484 GHz $Si^{18}O$ line at different offset positions, z, from the disk mid-plane (Fig. 1a). The position–velocity diagrams at $z \approx \pm 25$ au show velocity gradients similar to that along the mid-plane (Fig. 2a,c). As

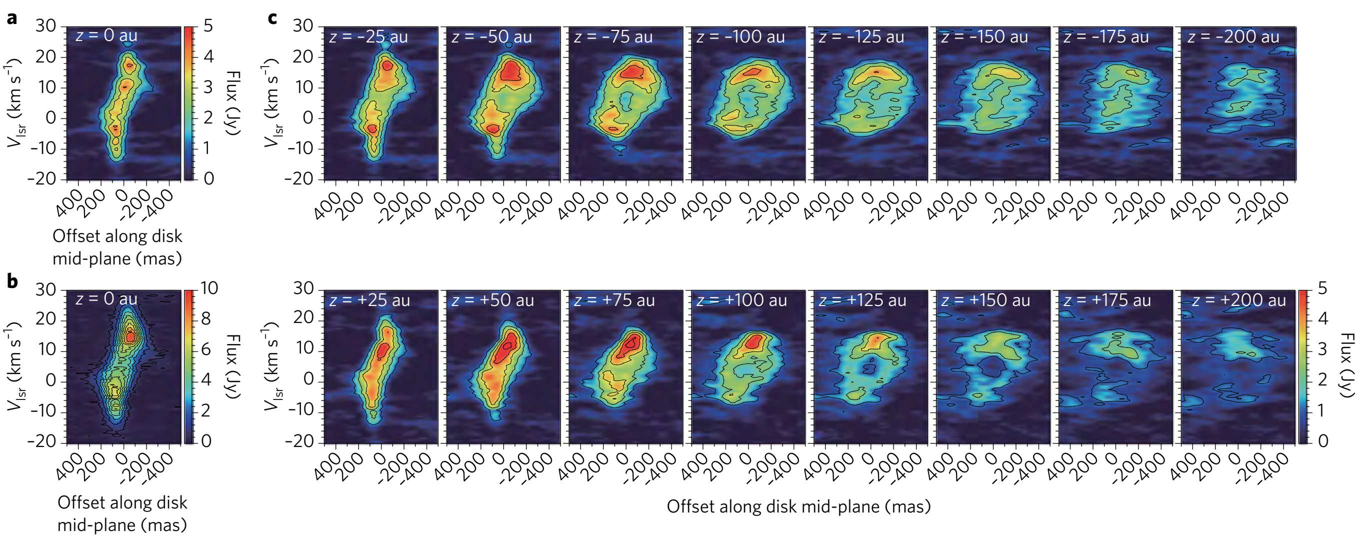

Figure 2 | Position–velocity diagrams parallel to the disk mid-plane. **a**, 484 GHz $Si^{18}O$ line at the offset $z = 0$ au (mid-plane). Contour levels are 3, 6, 12, 24, … times the r.m.s. noise level of 358 mJy. **b**, 463 GHz H_2O line at the offset $z = 0$ au (mid-plane). Contour levels are 3, 6, 12, 24, … times the r.m.s. noise level of 166 mJy. **c**, Same as **a**, but at different offset positions from $z = \pm 25$ au to ± 200 au with an interval of 25 au, as shown in Fig. 1a. Contour levels are the same as in **a**, but with different r.m.s. noise levels of 310–390 mJy for each position offset. The vertical axes represent the line-of-sight velocity with respect to the local standard of rest (lsr).

a result of the beam size of 50 au, which is larger than the 25 au width and interval of the position–velocity diagram slices, the data could be affected by contamination from the disk mid-plane. However, elliptical structures in the position–velocity diagram with a slight inclination become clearer at $z = \pm 75$ au or larger distances from the mid-plane. These can be interpreted as rotation with radial expansion perpendicular to the outflow axis (Supplementary Fig. 1d). Such a clear and continuous structural change in the position–velocity diagrams of the outflow directly connecting from the disk with rotation and radial expansion is revealed here for the first time. It is a major difference from previous maser observations, which could measure proper motions at higher angular resolution, but with discrete sampling of the spatial structures[6,7]. These findings are facilitated by utilizing high excitation thermal emission from the H_2O and $Si^{18}O$ lines.

Position–velocity diagrams along the outflow axis show the detailed structure of the outflow as a function of the distance from the disk mid-plane (see Methods; Fig. 3). R_{in} and R_{out} increase at larger offsets from the mid-plane (Fig. 3a). The radial expansion velocity perpendicular to the outflow axis, $v_r(r = R_{out}) \approx 10\,km\,s^{-1}$ shows no significant trend as a function of the distance from the disk mid-plane (Fig. 3b). In contrast, the rotation velocities at both of the inner $v_\varphi(r = R_{in})$ and outer $v_\varphi(r = R_{out})$ radii are almost constant close to the mid-plane within $|z| \leq 50$ au, whereas those at the outer radius slow down significantly at larger offsets from the mid-plane (Fig. 3c). The specific angular momentum, $J = v_\phi r$, of the outflow is almost constant within $|z| \leq 50$ au, particularly for the inner radius R_{in}, although there is still a significant amount of specific angular momentum at the larger distance from the disk mid-plane (Fig. 3d). Given the enclosed mass of 8.7 $M_\odot$ and the conservation of angular momentum, the specific angular momentum of 400–600 au km s^{-1} corresponds to centrifugal radii of 21–47 au, where the gravitational and centrifugal forces balance. The derived centrifugal radii agree with that of the observed disk size (Fig. 3a), implying that the outflow mainly originates in a region close to the derived centrifugal radii. Such a rotating outflow launched in the disk outer radii is most likely explained by the magneto-centrifugal disk wind mechanism, adding strong support to previous claims[6,11]. Similarly, the launching radii of magneto-centrifugal disk winds in low-mass YSOs are also comparable to their disk radii, as seen in recent ALMA observations of TMC-1A[25]. The centrifugal radii and specific angular momentum in Source I are larger than those of TMC-1A due to its larger stellar mass. We note that the specific angular momentum at the outer radius R_{out} shows a slightly decreasing trend as the outflow moves away from the disk mid-plane (Fig. 3d), which contrasts with the trend seen in TMC 1A[25]. This is probably due to the dissipation of angular momentum from the outflow to the ambient gas or the contribution from the ambient gas with smaller angular momentum swept up by the outflow in Source I. The opening angle of the outflow (Supplementary Fig. 4) has a maximum value of 70° close to the mid-plane $z = \pm 25$ au (Fig. 3e). Such a wide opening angle close to the launching point and collimation at a larger distance, which could be achieved by hoop stress[3], are also indicative of a magneto-centrifugal disk wind.

The dynamical timescale (t_{dyn}) of the outflow traced by the $Si^{18}O$ line is estimated from the outer radius and radial expansion velocity, $t_{dyn} = R_{out}/v_r = 70 \pm 4$ yr (1σ) at $z = \pm 150$ au. It should be noted that the $Si^{18}O$ line traces only the central part of the larger northeast–southwest bipolar outflow with a much longer dynamical timescale[16]. Using this dynamical time, the outward velocity along the outflow axis, v_z, is estimated to be 10 km s^{-1}. This is close to the three-dimensional velocity of the low-velocity '18 km s^{-1}' outflow measured by the proper motions of H_2O masers[6], but much lower than those observed in optical jets driven by T-Tauri stars[5]. The three-dimensional velocity of 18 km s^{-1} is consistent with the maximum rotation velocity in the disk mid-plane of 17.9 km s^{-1} at $R_{in}(z = 0) = 24$ au. The similarity lends further support to our inferred outflow launching radius. Using the derived enclosed mass (8.7 $M_\odot$) and outward velocity along the outflow (10 km s^{-1}), we can also derive the launching radii of the outflow using the magneto-centrifugal disk wind model[26] (their equation (4)). The calculated values, 5–25 au, are comparable to or slightly smaller than the centrifugal radii as estimated here (21–47 au). If we instead adopt an outward velocity of 18 km s^{-1} from maser kinematics[6], the estimated launching radii become smaller by 10–25%. Alternative outflow mechanisms include the entrainment of ambient gas by a high-velocity (>100 km s^{-1}) primary jet[8]. However, the kinematics discussed here are better explained by an outflow directly driven by a disk wind, rather than entrainment by a narrow high-velocity jet, which has never been identified towards Source I. The launching radius estimated here suggests that contributions from other mechanisms (stellar wind[9] or X-wind[10], which are launched from a close vicinity to the central YSO) would be small for Source I.

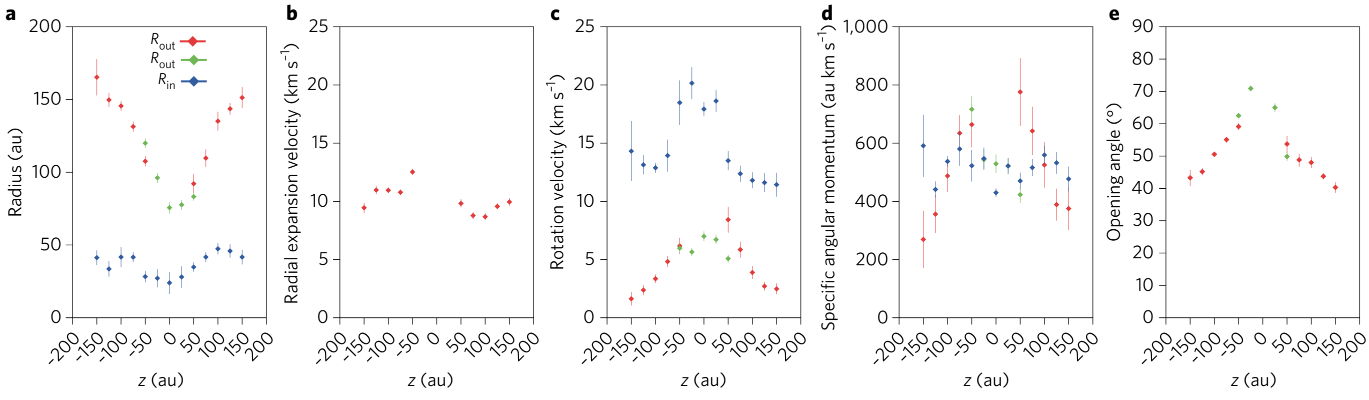

Figure 3 | Derived outflow parameters from position–velocity diagrams of the 484 GHz $Si^{18}O$ line. a, Outer and inner radii, R_{out} and R_{in}, of the outflow/disk. **b**, Radial expansion velocity perpendicular to the outflow axis at the outer radius, $v_r(R_{out})$. **c**, Rotation velocity at the outer and inner radii, $v_\phi(R_{out})$ and $v_\phi(R_{in})$. **d** Specific angular momentum at the outer and inner radii, $J(R_{out})$ and $J(R_{in})$. **e**, Opening angle of the outflow θ (Supplementary Fig. 4). The fitting results to the linear velocity gradients across the outer radius (green) are plotted for the offset within $|z| \leq 50$ au from the mid-plane, while those of the inner radius (blue) are plotted for all the offset positions of z. The fitting results to the elliptical function (red) are plotted for the offset of $|z| \geq 50$ au or larger from the mid-plane. Note that both linear and elliptical function fitting are performed at $z = \pm 50$ au for comparison (see Methods). All the error bars (1σ) are estimated from error propagation from the fitting on position–velocity diagrams.

In Orion KL, high-velocity (~100 km s^{-1}) explosive outflows have been identified in infrared and radio observations, which are thought to have been triggered by a dynamical encounter event 500 years ago[27,28]. It is predicted that Source I is a binary system that was newly formed during the encounter event with a total mass and binary separation of 20 $M_\odot$ and <10 au, respectively[23,27] (although the mass, luminosity and temperature of the central star or binary system is still controversial[13,14,19,21,23,29]). Even if we assume a higher mass (20 $M_\odot$) and a binary system, the corresponding centrifugal radii, 9–20 au, would not conflict with a magneto-centrifugal disk wind driven by a circumbinary disk[30]. Thus our results provide a compelling observational signature of a rotating outflow driven by the magneto-centrifugal disk wind launched by a high-mass YSO candidate, Source I. This picture is analogous to those of low-mass YSOs[25] in which mass accretion occurs through disks by carrying away significant amounts of angular momentum by the magneto-centrifugal disk wind, as predicted by theoretical models[1–4]. This study shows not only the outflow driving mechanism, but also proves a possible scenario of mass accretion and angular momentum transfer processes in high-mass star formation via disk accretion.

Methods

ALMA observations and data analysis. Observations of the submillimetre $Si^{18}O$ and H_2O lines were carried out with the ALMA on 27 July 2015 (490 GHz) and 27 August 2015 (460 GHz) as one of the science projects in cycle 2 (2013.1.00048). The target source was the radio Source I in Orion KL (Orion Source I) and the tracking centre position was right ascension (J2000) = 05 h 35 m 14.512 s, declination (J2000) = −05° 22′ 30.57′′. The total on-source integration time of the target source was 410 and 315 s for 463 and 484 GHz, respectively. The vibrationally ground $Si^{18}O$ line at 484.056 GHz (J = 12–11, E_l = 128 K[31], where E_l is the lower state energy) and the vibrationally excited H_2O line at 463.171 GHz ($\nu_2 = 1$, $J_{K_a,K_c} = 4_{2,2}–3_{3,1}$, E_l = 2,744 K[32]) in ALMA band 8 were selected for this study. The primary flux calibrator, bandpass calibrator and secondary gain calibrator were J0423−013, J0522−3627 and J0607−0834, respectively. The array consisted of 41 and 40 antennas, each with a diameter of 12 m in the configuration with the maximum baseline length of 1466.2 and 1574.4 m for 484 and 463 GHz, respectively. The primary beam size was 12.05′′. The median system noise temperature was around ~400 K at both frequency bands. The ALMA correlator provided the four spectral windows with total bandwidths of 1875 and 937.5 MHz for the 484 GHz $Si^{18}O$ and 463 GHz H_2O lines, respectively. The channel spacings of the spectrometers were 976.562 and 488.281 kHz for the 484 GHz $Si^{18}O$ and 463 GHz H_2O lines, respectively, which corresponds to velocity spacings of 0.6 and 0.3 km s^{-1}, respectively.

The synthesis imaging and self-calibration were carried out with the Common Astronomy Software Applications (CASA) software package (https://casa.nrao.edu/). We used the calibrated data delivered by the East-Asia ALMA Regional Center. First, the visibility data were separated into spectral lines and continuum emissions by setting the line-free channels with the CASA task 'uvcontsub'. Next, both phase and amplitude self-calibration were performed with the continuum emission of Source I by integrating over all the channels using the CASA tasks 'clean' and 'gaincal'. As a result of calibration problems in the delivered data due to the large atmospheric opacity around 487 GHz, we used only three spectral windows among four ALMA basebands to make a continuum image at 490 GHz[22]. The phase and amplitude solutions of self-calibration were applied to all the spectral channels, including the target lines, by the CASA task 'applycal'. The uniform-weighted synthesized images were made for both the 484 GHz $Si^{18}O$ and 463 GHz H_2O lines using the CASA task 'clean', providing velocity channel maps (image cubes; Supplementary Fig. 5). The resultant synthesized beam sizes were 124 mas × 97 mas with the position angle of 73.3° at 484 GHz and 121 mas × 104 mas with the position angle of 85.2° at 463 GHz. The maps of the 484 GHz $Si^{18}O$ and 463 GHz H_2O lines were registered with that of the 460 and 490 GHz continuum maps, respectively[22]. The moment maps were created by the CASA task 'immoments'. Some of the analysis and plotting were performed with the Astronomical Image Processing System (AIPS) software package (www.aips.nrao.edu). We made position–velocity diagrams using AIPS in a standard manner.

The position–velocity diagrams were analysed to derive the physical parameters by fitting the images. We found that the observed position–velocity diagrams show different velocity structures (Fig. 2c). These position–velocity diagrams can be interpreted as a combination of rotation and radial expansion motions perpendicular to the outflow axis. Schematic model position–velocity diagrams are shown in Supplementary Fig. 1. If the slice of the rotating outflow or disk has a ring-like structure with a central hole, we can see a linear velocity gradient without the high-velocity components associated with the inner part. If the gas radially expands outwards with significant rotation, the position–velocity diagram shows an elliptical morphology with velocity gradients.

To derive the radius of the outflow, the rotation velocity and the radial expansion velocity, we fitted the linear function or elliptical function to the position–velocity diagrams (Supplementary Fig. 1). Examples are shown in Supplementary Figs 2 and 3. We determined the peak position and those of the full-width at half-maximum (FWHM) for each velocity channel by Gaussian fits to the intensity profile (Supplementary Figs 2c and 3c). The linear velocity gradient was applied to the position–velocity diagrams within $z = \pm 50$ au or smaller offset from the disk mid-plane. For the position–velocity diagrams with an elliptical shape, we used two Gaussian fits to determine the double-peaked intensity profiles if there were two peak positions at the same velocity channel (Supplementary Fig. 3c). The elliptical function fitting was conducted for the position–velocity diagrams at an offset of $z = \pm 50$ au or larger distance from the disk mid-plane. For comparison, we applied both fitting procedures at $z = \pm 50$ au. To derive linear velocity gradients across the disk inner radius, we carried out fitting to use the highest velocity components with the width of six channels (3 km s^{-1}), as shown in Supplementary Figs 2a and 3a. The linear velocity gradients across the disk outer radius were obtained by fitting the linear function using the outermost part corresponding to the FWHM positions with a velocity width of 3 km s^{-1} (or six channels), as shown in Supplementary Fig. 2b. To fit the elliptical-shaped position–velocity diagrams, we only used the outer boundary corresponding to the FWHM positions in the fit (Supplementary Fig. 3b). The quoted uncertainties for the peak positions and half-maximum positions were estimated from the fitting errors to the position–velocity diagrams at the 1σ level.

Using these fitting results, we estimated the outflow parameters, such as R_{in} and R_{out}, the radial expansion velocity perpendicular to the outflow axis, v_r, and the rotation velocity, v_ϕ, as a function of the distance from the disk mid-plane, z. The geometry of the outflow and the coordinate system used is illustrated in Supplementary Fig. 4. All the uncertainties for outflow parameters are estimated by those of the fitting of the position–velocity diagrams. We note that the fitting procedures discussed here are too simplified and hence further modelling, including multi-transition radiative transfer calculations, are required to discuss the derived parameters and rotation curves more quantitatively.

Data availability. The data that support the plots within this paper and other findings of this study are available from the corresponding author upon reasonable request. This paper makes use of the following ALMA data: ADS/JAO. ALMA#2013.1.00048.S.

Received 13 January 2017; accepted 27 April 2017; published 12 June 2017

References

1. Blandford, R. D. & Payne, D. G. Hydromagnetic flows from accretion discs and the production of radio jets. *Mon. Not. R. Astron. Soc.* **199,** 883–903 (1982).
2. Tomisaka, K. The evolution of the angular momentum distribution during star formation. *Astrophys. J. Lett.* **528,** L41–L44 (2000).
3. Pudritz, R. E., Ouyed, R., Fendt, C. & Brandenburg, A. in *Protostars and Planets V* (eds Reipurth, B. *et al.*) 277–294 (Univ. Arizona Press, 2007).
4. Machida, M. N. Protostellar jets enclosed by low-velocity outflows. *Astrophys. J. Lett.* **796,** L17 (2014).
5. Belloche, A. in *Role and Mechanisms of Angular Momentum Transport During the Formation and Early Evolution of Stars* (eds Hennebelle, P. & Charbonnel, C.) 25–66 (EAS Publications Series, EDP Sciences, 2013).
6. Greenhill, L. J., Goddi, C., Chandler, C. J., Matthews, L. D. & Humphreys, E. M. L. Dynamical evidence for a magnetocentrifugal wind from a 20 $M_\odot$ binary young stellar object. *Astrophys. J. Lett.* **770,** L32 (2013).
7. Burns, R. A. *et al.* A 'water spout' maser jet in S235AB-MIR. *Mon. Not. R. Astron. Soc.* **453,** 3163–3173 (2015).
8. Arce, H. G. *et al.* in *Protostars and Planets V* (eds Reipurth, B. *et al.*) 245–260 (Univ. Arizona Press, 2007).
9. Bouvier, J. *et al.* in *Protostars and Planets VI* (eds Beuther, H. *et al.*) 433–450 (Univ. Arizona Press, 2014).
10. Shu, F. *et al.* Magnetocentrifugally driven flows from young stars and disks. 1: A generalized model. *Astrophys. J.* **429,** 781–796 (1994).
11. Matthews, L. D. *et al.* A feature movie of SiO emission 20–100 au from the massive young stellar object Orion Source I. *Astrophys. J.* **708,** 80–92 (2010).
12. Kim, M. K. *et al.* SiO maser observations toward Orion-KL with VERA. *Publ. Astron. Soc. Jpn* **60,** 991–999 (2008).
13. Menten, K. M. & Reid, M. J. What is powering the Orion Kleinmann-Low infrared nebula? *Astrophys. J. Lett.* **445,** L157–L160 (1995).
14. Reid, M. J., Menten, K. M., Greenhill, L. J. & Chandler, C. J. Imaging the ionized disk of the high-mass protostar Orion I. *Astrophys. J.* **664,** 950–955 (2007).
15. Testi, L., Tan, J. C. & Palla, F. The near-infrared reflected spectrum of Source I in Orion-KL. *Astron. Astrophys.* **522,** A44 (2010).
16. Plambeck, R. L. *et al.* Tracing the bipolar outflow from Orion Source I. *Astrophys. J. Lett.* **704,** L25–L28 (2009).

17. Zapata, L. A. *et al.* ALMA observations of the outflow from Source I in the Orion-KL region. *Astrophys. J. Lett.* **754,** L17 (2012).
18. Hirota, T., Kim, M. K. & Honma, M. The first detection of the 232 GHz vibrationally excited H_2O maser in Orion KL with ALMA. *Astrophys. J. Lett.* **757,** L1 (2012).
19. Hirota, T., Kim, M. K., Kurono, Y. & Honma, M. A hot molecular circumstellar disk around the massive protostar Orion Source I. *Astrophys. J. Lett.* **782,** L28 (2014).
20. Hirota, T., Kim, M. K. & Honma, M. ALMA observation of the 658 GHz vibrationally excited H_2O maser in Orion KL Source I. *Astrophys. J.* **817,** 168 (2016).
21. Plambeck, R. L. & Wright, M. C. H. ALMA observations of Orion Source I at 350 and 660 GHz. *Astrophys. J.* **833,** 219 (2016).
22. Hirota, T. *et al.* ALMA band 8 continuum emission from Orion Source I. *Astrophys. J.* **833,** 238 (2016).
23. Goddi, C., Humphreys, E. M. L., Greenhill, L. J., Chandler, C. J. & Matthews, L. D. A multi-epoch study of the radio continuum emission of Orion Source. I. Constraints on the disk evolution of a massive YSO and the dynamical history of Orion BN/KL. *Astrophys. J.* **728,** 15 (2011).
24. Tercero, B., Vincent, L., Cernicharo, J., Viti, S. & Marcelino, N. A line-confusion limited millimeter survey of Orion KL. II. *Silicon-bearing species. Astron. Astrophys.* **528,** A26 (2011).
25. Bjerkeli, P., van der Wiel, M. H. D., Harsono, D., Ramsey, J. P. & Jorgensen, J. K. Resolved images of a protostellar outflow driven by an extended disk wind. *Nature* **540,** 406–409 (2016).
26. Anderson, J. M., Li, Z.-Y., Krasnopolsky, R. & Blandford, R. D. Locating the launching region of T Tauri winds: the case of DG Tauri. *Astrophys. J. Lett.* **590,** L107–L110 (2003).
27. Bally, J. *et al.* Explosive outflows powered by the decay of non-hierarchical multiple systems of massive stars: Orion BN/KL. *Astrophys. J.* **727,** 113 (2011).
28. Zapata, L. A., Schmid-Burgk, J., Ho, P. T. P., Rodríguez, L. F. & Menten, K. M. Explosive disintegration of a massive young stellar system in Orion. *Astrophys. J. Lett.* **704,** L45–L48 (2009).
29. Chatterjee, S. & Tan, J. C. Gravitational slingshot of young massive stars in Orion. *Astrophys. J.* **754,** 152 (2012).
30. Machida, M. N., Inutsuka, S.-I. & Matsumoto, T. The circumbinary outflow: a protostellar outflow driven by a circumbinary disk. *Astrophys. J. Lett.* **704,** L10–L14 (2009).
31. Müller, H. S. P., Schlöder, F., Stutzki, J. & Winnewisser, G. The Cologne Database for Molecular Spectroscopy, CDMS: a useful tool for astronomers and spectroscopists. *J. Molec. Struct.* **742,** 215–227 (2005).
32. Pickett, H. M. *et al.* Submillimeter, millimeter, and microwave spectral line catalog. *J. Quant. Spectrosc. Radiat. Transfer* **60,** 883–890 (1998).

Acknowledgements

We are grateful to R.L. Plambeck, Y. Oya, N. Sakai and S. Yamamoto for valuable discussions. The ALMA is a partnership of the European Southern Observatory (representing its member states), the National Science Foundation (USA) and the National Institutes of Natural Sciences (Japan), together with the National Research Council Canada, National Science Council of Taiwan and Academia Sinica Institute of Astronomy and Astrophysics (Taiwan) and the Korea Astronomy and Space Science Institute (Republic of Korea), in cooperation with the Republic of Chile. The Joint ALMA Observatory is operated by the European Southern Observatory, Associated Universities Inc. (AUI)/National Radio Astronomy Observatory and the National Astronomical Observatory of Japan (NAOJ). We thank the staff at ALMA for making the observations and reducing the data. T.H. is supported by the Ministry of Education, Culture, Sports, Science and Technology (MEXT)/Japan Society for the Promotion of Science (JSPS) KAKENHI grant numbers 21224002, 24684011, 25108005 and 15H03646 and the ALMA Japan Research Grant of the NAOJ Chile Observatory, NAOJ-ALMA-0006, -0028 and -0066. M.N.M. is supported by MEXT/JSPS KAKENHI grant numbers 15K05032 and 17K05387. K.M. is supported by MEXT/JSPS KAKENHI grant number 15K17613. M.H. is supported by MEXT/JSPS KAKENHI grant numbers 24540242 and 25120007. Data analyses were in part carried out on the common use data analysis computer system at the Astronomy Data Center, NAOJ.

Author contributions

T.H. led the project as a principal investigator of the ALMA observations and performed the data analysis. M.N.M. and Y.M. interpreted the ALMA results from the theoretical point of view. K.M. analysed part of the ALMA data and checked the results. N.M., M.K.K., R.A.B. and M.H. contributed to writing the paper. All the authors discussed the results and commented on the paper.

Additional information

Supplementary information is available for this paper.

Reprints and permissions information is available at www.nature.com/reprints.

Correspondence and requests for materials should be addressed to T.H.

How to cite this article: Hirota, T. *et al.* Disk-driven rotating bipolar outflow in Orion Source I. *Nat. Astron.* **1,** 0146 (2017).

Publisher's note: Springer Nature remains neutral with regard to jurisdictional claims in published maps and institutional affiliations.

Competing interests

The authors declare no competing financial interests.